

Contents

Table of Contents	i
List of Figures	i
List of Tables	iii
0.1 Coupling Nanodiamonds to Optical Antennas	1
0.1.1 Plasmonic Antennas	1
0.1.2 Plasmonic Antenna Design and Simulation	3
0.1.3 SiV center in a Plasmonic Double Bowtie Antenna	5
0.2 Antennas	6
0.2.1 Plasmonic Antennas	6
0.2.2 Plasmonic Antenna Design	11
0.2.3 SiV centers in a Plasmonic Double Bowtie Antenna	12
Index	17

List of Figures

1	Schematic of a double bowtie antenna	2
2	Hot-spot of a double bowtie antenna	3
3	SEM images of double bowtie structures.	4
4	Simulation of the resonance spectrum of a double bowtie antenna	5
5	Pick and Place technique for nanodiamond manipulation, nanodiamond colored blue in the image for better visibility. (a) A nanodiamond sticking to the nanomanipulator tip which was lifted off the substrate (b) Transfer of the nanodiamond to the target antenna structure which is in the background.	7
6	SEM detail image of the middle of the double bowtie antenna structure with the transferred nanodiamond. Vor better visibility, the nanodiamond is colored blue. Antenna damage caused by the placement of the nanodiamond is visible as black area at the tip of the top triangle	7
7	SEM images of the antenna structures. (a) Overview of a field of antenna structures exhibiting various dimensions. (b) Detail of one antenna sturcture. In the middle the double bowtie design is visible. The ring grating structure is surrounding it.	10
8	CCD image recorded in the confocal setup of an antenna structure under white light illumination. In the middle, the nanodiamond containing multiple SiV centers had been placed.	10
9	FDTD calculations of the electric field intensity as a function of wavelength in the gap of a double bowtie nanoantenna containing a nanodiamond.	11
10	CCD image recorded in the confocal setup of an antenna structure under white light illumination. In the middle, the nanodiamond containing multiple SiV centers had been placed.	13
11	(a) Picture recorded with a commercial high resolution laser scanning microscope. The area shaded in blue represents the photoluminescence scan in image (b). (b) Photoluminescence scan of a $8\text{ }\mu\text{m} \times 13\text{ }\mu\text{m}$	14
12	(a) PL spectrum of the emitter in the preselected nanodiamond at room temperature. Black: experimental results; red: fit to experimental data, verfnuenftige fehlergrenzen einfuegen which yields a ZPL center wavelength of $738.55(1)\text{ nm}$ and a linewidth of $5.09(3)\text{ nm}$	15

13	(a) Confocal scan of the double bowtie antenna where a nanodiamond containing multiple SiV centers had been placed. The rings are visible. (b) Detail scan of the triangles of the same antenna structure, which make up the double bowtie antenna. While the separate triangle cannot be seen, some edges and two bright spots are visible. To identify the place of the nanodiamond we compare the middle point of the rings in (a), the point of intersection of the edges and the bright spot and conclude that the upper bright spot in (b) is the location of the nanodiamond.	16
14	(a) Measured PL spectrum of the emitter after placing the nanodiamond into the nanoantenna, (b) Convolution of the spectrum of the measured PL spectrum of the emitter before pick-and-place (see Figure ??) and the simulated resonance spectrum of the nanoantenna (see Figure 9).	16
15	<caption>	17
16	<caption>	17
17	<caption>	18

List of Tables

0.1 Coupling Nanodiamonds to Double Bowtie Antenna Structures

Plasmonic nanoantennas are very recent devices designed to efficiently convert freely propagating optical radiation into localized energy and vice versa [?, ?, ?, ?, ?, ?]. Leveraging this unique property, integrating SiV centers with optical antennas creates coupled systems with a range of desirable features. These include enhanced photoluminescence emission and the ability to tailor photoluminescence spectra of the integrated emitters. The latter can be achieved by tuning the physical design parameters of the system including antenna geometry and emitter placement.

In this chapter we report on our efforts aimed at enhancing the properties of SiV centers by coupling them to optical double bowtie antennas. To this end we transfer selected nanodiamonds containing SiV centers to the target antenna structure using pick-and-place methods. After successful coupling we investigate the integrated structure experimentally. In addition to that we successfully relate some of our results to theoretical predictions.

In the following we give a short discussion of the most important properties of optical antennas. Then we sketch the actual coupling process and report on the optical properties of the resulting integrated structure.

0.1.1 Plasmonic Antennas

Optical nanoantennas act as converters between propagating and localized electro-magnetic fields. Thus, they can be used efficiently to couple photons in and out of nanoscale objects [?]. Due to their small physical sizes, comparable or smaller than the wavelength of visible light, they are capable of focusing optical fields to subdiffraction-limited volumes, offering the ability to manipulate electromagnetic fields at nanoscales [?, ?]. This property, dubbed sub-wavelength confinement, has successfully been exploited to enhance the excitation and emission of quantum emitters [?, ?, ?, ?] and to modify their spectra [?]. Resulting practical applications include near-field optical microscopy [?], surface enhanced spectroscopy [?, ?] and molecular sensing [?].

A nanoantenna is a nanostructure made from materials such as noble metals like gold or silver. These metals have in common that they are very susceptible to being polarized by electromagnetic fields. When illuminated by the incident electromagnetic radiation causes electrons in the metal to behave as a plasma that tends to move with respect to the atomic lattice. As a result excess charge at the opposite surfaces of the material accumulates and the material becomes temporarily polarized until restoring forces equilibrate the charge distribution.

Thus incident light of a given frequency induces oscillations in the free electron gas density in the surface layers of the metal. At resonance these light-induced oscillations exhibit modes of standing waves. The quasi-particles associated with these modes are known as localized surface plasmons (LSPs). For an in-depth treatment of LSPs in the context of nanoantennas we refer the reader to [?] and references therein.

Here it suffices to say, that LSPs facilitate the deciding property of optical antennas: Converting electromagnetic energy from the far-field into localized energy in the near-field. This

allows, in combination with the high collection-efficiencies of nanoantennas, to efficiently couple visible radiation with wavelengths of hundreds of nanometers, into small effective spatial volumes of only a few nanometer in diameter.

To create a controlled hot-spot several antenna designs are possible. In the context of this thesis we rely on double bowtie antennas available via a collaboration with N. Rahbany, group of C. Couteau, University of Technology of Troyes. Figure 1 illustrates the typical bowtie antenna.

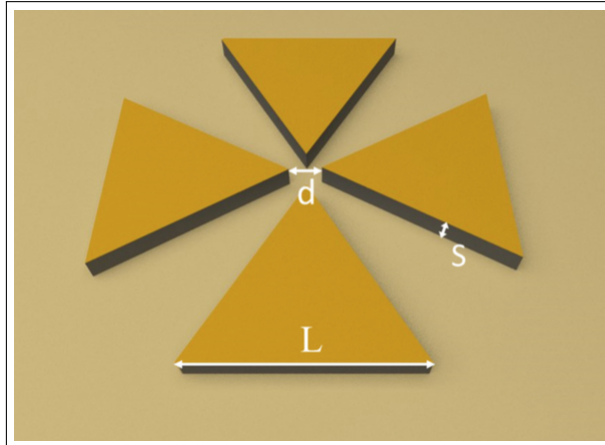


Figure 1: Schematic of a double bowtie antenna [?, ?, ?].

This antenna design utilizing a symmetric arrangement of four identical triangle-shaped blocks, separated by a small gap. This setup allows LSP modes local to individual blocks to couple with each other resulting in the formation of an intense hot-spot in the center area [?], see ?. The actual electromagnetic response of a double bowtie nanoantenna depends on its physical design parameters such as gap size, material used, geometry and size. Furthermore, properties of incident light such as wavelength and polarization determine antenna operation.

The improved electromagnetic field at the center of a metallic nanoantenna can be used to increase the spontaneous emission rate of emitters emitting at frequencies close to the resonance frequency of the antenna. This result is the known as Purcell effect [?]. The gap between the antenna arms acts as a resonant cavity providing a strong near field interaction with the emitter. This interaction modifies the density of states of the system, effectively providing additional modes for the emitter to decay into, thus amplifying its total decay rate. The amplification affects both radiative and non-radiative decay. The magnitude of the amplification for an emitter is quantified by the ratio of its enhanced decay rate to its free space decay rate, known as the Purcell factor F_p . This factor is proportional to Q/V_{eff} where Q denotes the quality of the antenna and V_{eff} the volume of the hot-spot. Thus antenna design must optimize F_p as a necessary condition for significant enhancement of fluorescence light emission.

In addition to the antennas local field enhancement, the emitters original quantum yield η_0 influences the overall effectiveness of the emission enhancement. From theoretical considerations [?, ?, ?, ?], the modified quantum efficiency η of the combined system consisting of

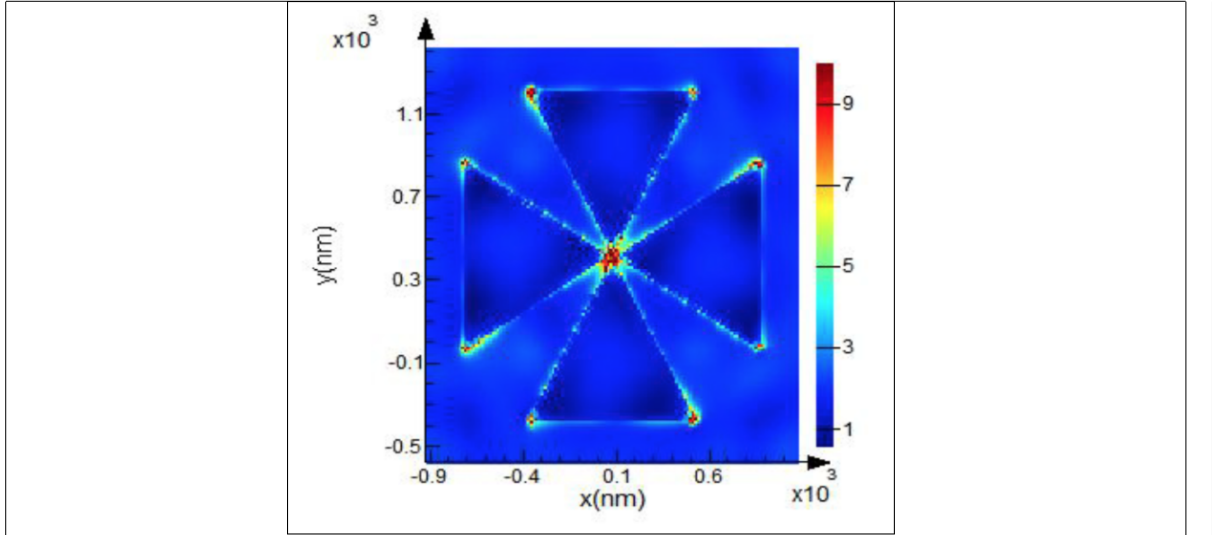


Figure 2: Simulation result of the electric field map of a gold double bowtie nanoantenna [?, ?, ?]. The structure has gap of $d = 150$ nm, a side length of $L = 2\text{ }\mu\text{m}$ and a thickness of $S = 60$ nm. The center of the antenna exhibits an area of pronounced focus, the so-called hot-spot.

emitter and antenna can be obtained as

$$\eta = \frac{\eta_0}{\frac{1-\eta_0}{F_p} + \frac{\eta_0}{\eta_{ant}}}, \quad (1)$$

where η_{ant} denotes the fraction of fluorescence light which is not dissipated through losses in the metal of the antenna. It is clear that an emitter with $\eta_0 \rightarrow 1$ will not profit from the Purcell effect. On the contrary, for realistic antennas with $\eta_{ant} < 1$ antenna-induced losses reduce the overall quantum yield η . Consequently poor emitters with low initial η_0 stand to profit the most from antenna-emitter coupling provided antennas are engineered well, i.e. they maximize their Purcell Factors and minimize their losses. For an in-depth review

The presented considerations illustrate that due to their relatively low quantum efficiency, SiV centers are excellent candidates for coupling with antennas. Thus it is promising to exploit the improved electromagnetic field at the center of a double bowtie antenna to enhance the spontaneous emission rate of SiV centers and thus improve their merit as single photon sources.

0.1.2 Plasmonic Antenna Design and Simulation

To couple SiV centers to optical antennas, we work with gold double bowtie antennas on a gold substrate. In comparison with triangular, or single bowtie antennas, double bowtie antennas offer significantly improved intensity enhancements. Antennas were provided by N. Rahbany, group of C. Couteau, University of Technology of Troyes in a joined effort to explore the possibilities of combining antennas with SiV centers. The antennas themselves were fabricated using electron beam lithography, a technique suitable to imprint predetermined patterns onto a suitable substrate with nanoscale resolution [?]. Figure 7a shows a SEM image

of an array of antenna structures of various sizes. In Figure 7b a detail of an individual double bowtie antenna is shown. It can be seen that the double bowtie antenna is placed in the center of another structure, a so-called bulls-eye antenna, consisting of multiple concentric gratings. When illuminated by a laser at a proper angle, the gratings excite surface plasmon polaritons (SPPs) which are directed towards the center of the structure. If a double bowtie antenna is present in the center, SPPs can interact with the LSPs of the double bow tie, leading to an even stronger localization of electromagnetic fields in the gap of the bowtie. While this interaction certainly merits exploration in the context of enhancing SiV centers, we omit the excitation of SPPs in our first exploration of the coupling of SiV centers and antennas. Thus the presence of the gratings can be ignored for our purposes. The reader interested in the details of bulls-eye antennas and their properties is referred to [?].

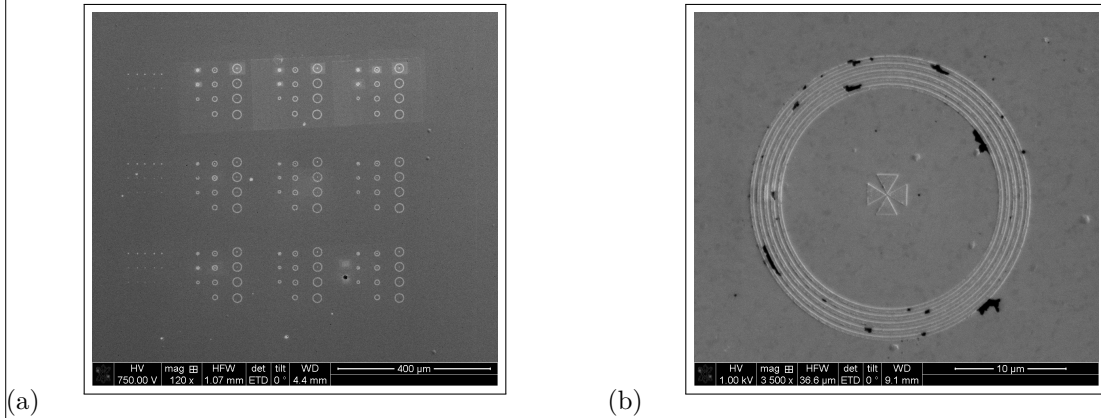


Figure 3: SEM images of antenna structures. (a) Overview of a field of antenna structures exhibiting various dimensions. (b) Detail of one antenna structure. In the middle the double bowtie design is visible. A grating structure consisting of multiple gratings is surrounding it.

To effectively enhance the emission of an emitter by coupling it to an optical antenna, the emission wavelength must match the resonant wavelength of the antenna. In the context of SiV centers a value of 738 nm is required. Since this value can be considered constant, the design parameters of the antenna must be chosen such, that the resulting resonance matches it. An additional constraint is placed on the size of the antenna gap, since it must be big enough to accommodate nanodiamonds hosting SiV centers, the former are around 100 nm in size. However, it cannot be chosen arbitrarily big, since bigger gaps lead to larger effective volumes and thus smaller Purcell Factors.

Using finite difference time domain (FDTD) simulation deploying Lumerical Software the design space of gold double bowtie nanoantennas on a gold substrate was explored [?]. Although we initially attempted to simulate antennas without a nanodiamond present in the gap, it was subsequently discovered that its ab initio inclusion yielded superior results. Thus to determine usable design parameters for our purposes, an integrated system combining antenna and nanodiamond was used. To better mimic experimental conditions and associated imperfections, the nanodiamond was placed slightly off-center in the gap.

In a series of simulations it was established that a gap size of $d = 150$ nm, a side length of $L = 2$ μm and a structure thickness of $S = 60$ nm are feasible parameters as referred to in [?]. The simulation required the index of refraction for gold which was taken from Palik [?, ?, ?, ?].

The resulting geometry hosting a nanodiamond is capable of producing a suitable hotspot when excited.

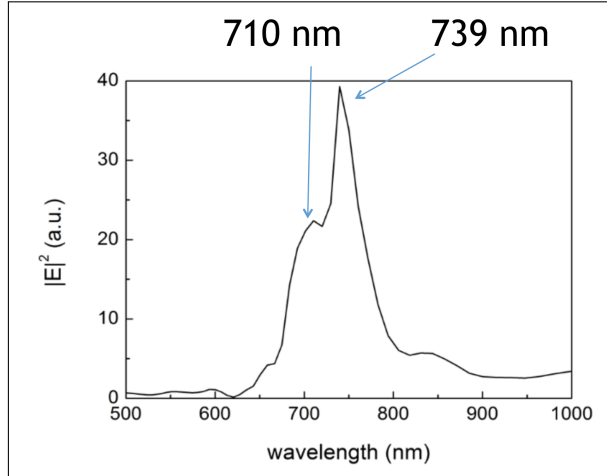


Figure 4: FDTD simulation of the electric field intensity of a double bowtie nanoantenna as a function of the wavelength of incident light. Two peaks are identified. The major peak corresponds exceptionally well with SiV center emission at 738 nm. The minor peak is attributed to the presence of a nanodiamond.

Finally, to pin-point the resonant wavelength for the antenna hosting a nanodiamond, the electric field intensity is simulated as a function of the wavelength of the incident light. The resulting spectrum is shown in Figure 4. Two resonant peaks are found. The intense major peak at 739 nm coincides exceptionally well with the SiV center emission wavelength 738 nm indicating successful antenna design. In addition to the major peak, an additional minor mode at a lower wavelength of 710 nm is found [?]. We remark that if the nanodiamond in the gap of the antenna is removed from the simulations, the minor feature vanishes. Thus the additional peak is well-attributed to the presence of the nanodiamond.

In summary, the combined simulation results suggest, that the engineered system of nanoantenna and nanodiamond is well suited to effectively enhance the emission from an SiV center hosted in the nanodiamond. In the following sections we report on the experimental realization of this preposition.

0.1.3 SiV center in a Plasmonic Double Bowtie Antenna

In the following we report on our attempts to couple SiV centers to double bowtie antennas. Given ideal nanodiamonds containing exactly one SiV center each, the major challenge of coupling consists of transporting a given nanodiamond to the gap of an antenna. However, nanodiamonds rarely contain exactly one SiV center. The identification of a perfect candidate requires manual examination of hundreds of nanodiamonds, making it an extremely tedious, error-prone and time-consuming process. In addition to that, methods such as pick-and-place entail a very real risk of permanently damaging or invalidating a precious candidate in transit to the antenna, thus rendering the significant efforts invested in identifying the candidate futile. In contrast to that, nanodiamonds containing anything from a small number to an entire ensemble of SiV centers are much more likely and thus easier to identify and to use.

Thus we approach the problem of coupling SiV centers to antennas in several phases. In the first phase nanodiamonds containing an entire ensemble of SiV centers are utilized. Such nanodiamonds can be found with high probability. Due to the large number of individual emitters involved, they exhibit an increased resilience against being damaged. The disadvantage is that once placed in the antenna, the whole ensemble will be affected by Purcell enhancement and as a result its effectiveness for individual emitters cannot be obtained.

After gaining experience in the first phase, the second phase aims at using nanodiamonds with a very low number of SiV centers hosted. Here the goal is to identify a candidate nanodiamond in a reasonable amount of time. Once transferred to an antenna using pick-and-place methods, saturation and second order correlation measurements can be attempted provided the involved emitters remain stable.

The third and last phase focuses on identifying a nanodiamond hosting a singleton SiV center building onto of the insights gained in the previous phases. After successful pick-and-place transit, a precise characterization of the emitter and its antenna-induced Purcell enhancement should be possible.

Here we report on our obtained results regarding phases one and two. At the time of writing this, phase three was not yet implemented.

0.2 Coupling Nanodiamonds to Double Bowtie Antenna Structures

In this chapter, the integration of SiV centers in nanodiamonds with double bowtie nanoantenna structures is presented. The emission from the coupled system has two advantages:

- The antenna causes an enhancement in the SiV center's photoluminescence emission intensity.
- The photoluminescence spectrum of the nanodiamond is modified depending on the geometry of the nanoantenna as well as the position of the emitter in the gap. This provides the flexibility of designing the nanoantennas to accurately predict and tune the emitters' PL spectrum as desired.

0.2.1 Plasmonic Antennas

nancy Doktorarbeit: Plasmons can be considered as a collective oscillation of the free electron density on the surface of a conducting material.

Localized surface plasmons (LSP) are the result of stationary resonant oscillations of the surface charge density at the boundaries of metallic nanostructures [37,38]. Due to their significant optical properties, LSPs are shown to enhance electromagnetic field confinement.

Plasmonic nanoantennas have proven to be very successful candidates in tailoring light propagation and confinement at the nanoscale. Electromagnetic antennas are defined as metallic devices used for receiving and transmitting electromagnetic waves. In addition to acting as probing devices, antennas must also serve as directional devices that optimize and accentuate radiation energy in some directions and suppress it in others [77]. Optical nanoantennas benefit from their sizes, which are comparable to or smaller than the wavelength of visible

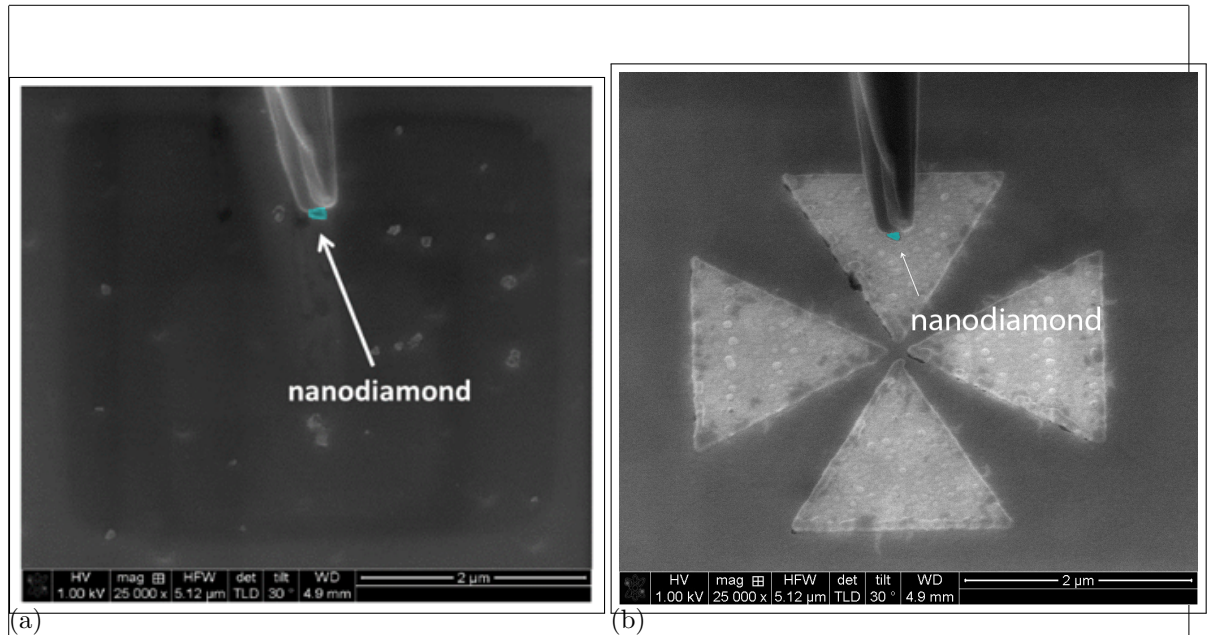


Figure 5: Pick and Place technique for nanodiamond manipulation, nanodiamond colored blue in the image for better visibility. (a) A nanodiamond sticking to the nanomanipulator tip which was lifted off the substrate (b) Transfer of the nanodiamond to the target antenna structure which is in the background.

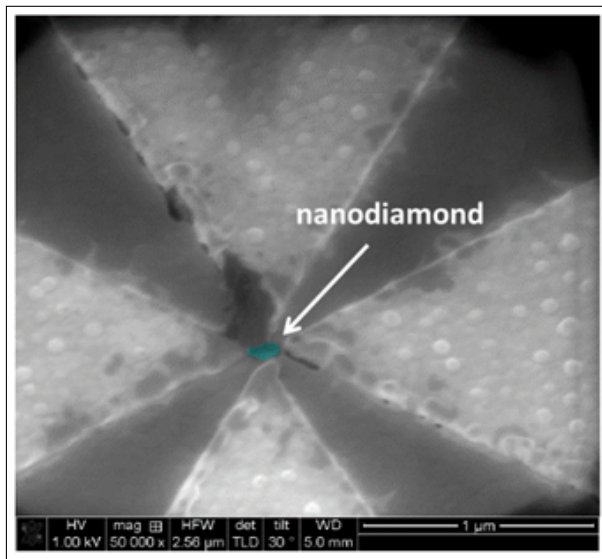


Figure 6: SEM detail image of the middle of the double bowtie antenna structure with the transferred nanodiamond. Vor better visibility, the nanodiamond is colored blue. Antenna damage caused by the placement of the nanodiamond is visible as black area at the tip of the top triangle

light, to overcome the diffraction limit and manipulate electromagnetic fields at the nanoscale [78]. This allows them to be widely used in many applications such as near-field optical microscopy [79], surface enhanced spectroscopy [80,81], sensing [82], medical therapy [83], and optoelectronic devices [84]. When light is incident on metallic nanoantennas, modes of standing waves are created at resonance. This creates an electric field enhancement in their vicinity. A good nanoantenna is characterized by its high collection efficiency (large cross section), and its ability to focus incident electromagnetic light into sub-wavelength areas (large near-field enhancement). To improve their performance, researchers have found that cutting a gap in the center of nanoantennas leads to a higher near-field enhancement while maintaining the same effective cross-section [85]. This occurs due to the coupling between the LSP modes of the two parts of the nanoantenna creating a hotspot in the gap. Exciting LSPs can be simply achieved by resonantly illuminating nanostructures with electromagnetic waves.

[?] Optical antennas, acting as converters between propagating and localized fields, provide an effective route to couple photons in and out of nanoscale objects. These antennas are the counterparts of conventional radio and microwave antennas and operate in the visible regime (1, 2). Optical antennas have been shown to focus optical fields to subdiffraction-limited volumes (3), enhance the excitation and emission of quantum emitters (4–7), and modify their spectra (8).

A characteristic of antennas is their directed emission and reception. So far, the control of directionality has mainly been pursued by photonic crystal structures (9) and surface-plasmon-based devices (10–12). However, for such structures approaching the nanometer scale diffraction can limit the collimated beaming of light. On the other hand, the interaction of quantum emitters with light is best enhanced with microcavities (13, 14). Compared with these approaches, plasmonic nanoantennas offer a much smaller footprint in an open geometry combining strong subwavelength fields and increased transition rates, together with the prospect of directionality.

[?] from gold, a metal that can develop charge oscillations in its surface layers when excited by optical radiation. These antennas allow visible radiation, which has wavelengths of hundreds of nanometers, to couple into a semiconductor quantum dot only a few nanometers in diameter, and also direct the emission

Good mode-matched antennas reradiate their energy after excitation within a single cycle of the wave. Molecules or quantum dots take nanoseconds or even longer to reradiate their energy. This time scale corresponds to about 1 million oscillations at optical frequencies, and the emission is in all directions.

If an atom, molecule, or quantum dot is placed into the near-field of a metallic nanoantenna (within about 1/50th the wavelength of the emitted radiation), its excited state can radiate photons very efficiently to free space (see the figure, panel B). The quantum emitters can emit a single photon, which can be exploited in quantum optics. Additionally, the nanoantenna can redirect radiation into a defined solid angle in space and impose a specific polarization on it.

The demonstration of the Purcell effect, which is the acceleration of the decay of the quantum emitter caused by impedance matching by the antenna to free space, could also enhance the radiative emission over nonradiative losses

[?] The electromagnetic antenna, originally referred to as an aerial, is a transducer between electromagnetic waves and electric currents, and generally operates in the radiofrequency regime. In analogy with the electromagnetic antenna, we define the optical antenna as a device that converts freely propagating optical radiation into localized energy, and vice versa. The spatial extent of a receiver or transducer is commonly much smaller than the

wavelength of radiation, \hat{L}_z , and is typically of the order of $\hat{L}_z/100$. Surface plasmon resonances make optical antennas particularly efficient at selected frequencies. A generic antenna problem is illustrated in Fig. 3. It consists of a transmitter and a receiver, both represented by dipoles p . The antenna is introduced to enhance the transmission efficiency from the transmitter to the receiver. This enhancement can be achieved by increasing the total amount of radiation released by the transmitter, for which the antenna efficiency is a useful figure of merit:

$$p = p \quad (2)$$

where P is the total power dissipated by the antenna, P_{rad} is the radiated power and P_{loss} is the power dissipated through other means, such as by absorption in the antenna. However, the transmission efficiency can also be improved by directing the radiation in the direction of the receiver. The efficiency for this process is represented by the directivity:

$$p = p \quad (3)$$

where the angles $\hat{\gamma}$ and $\hat{\tau}$ represent the direction of observation and $p(\hat{\gamma}, \hat{\tau})$ is the angular power density. The combination of antenna efficiency and directivity is referred to as the antenna gain:

$$p = p \quad (4)$$

By reciprocity, we can interchange the fields and sources in Fig. 3 to give $p_1 \cdot E_2 = p_2 \cdot E_1$, where E_1 (E_2) is the field of dipole p_1 (p_2) evaluated at the location of p_2 (p_1). A good transmitting antenna is therefore also a good receiving antenna. For a transmitter in the form of a two-state quantum emitter, reciprocity leads to a relationship between the emitter's excitation rate \dot{N}_{exc} and its spontaneous emission rate:

$$p = p \quad (5)$$

Here, the superscript \wedge refers to the absence of the antenna and the subscript \wedge indicates the polarization state; that is, the electric field vector points in direction of the $\hat{\gamma}$ unit vector. An equivalent equation holds for polarization in the $\hat{\tau}$ direction. Interestingly, excitation in a direction of high directivity allows the excitation rate to be enhanced more strongly than the radiative rate. Another important antenna parameter is the antenna aperture, which is formally the same as the absorption cross-section sigma. Let us consider a dipole-like receiver with a cross-section σ that is not coupled to an antenna. The unit vector in the direction of the absorption dipole axis is denoted as n_p and the incident field at the location of the receiver is E_0 . Once we couple the receiver to an antenna, the field at the receiver increases to E and the cross-section or antenna aperture becomes

$$p = p \quad (6)$$

Thus, the aperture of an optical antenna scales with the local intensity enhancement factor. Theoretical and experimental studies have shown that intensity enhancements of 10^4 – 10^6 are readily achievable^{14,36,37} and hence, for typical molecules with a free-space cross-sections of $\sigma = 1 \text{ nm}^2$, we find that a layer of molecules spaced 0.1 nm apart can absorb all of the incident radiation if each molecule is coupled to an optical antenna. Of course, this estimate ignores the coupling between antennas and therefore has limited validity.

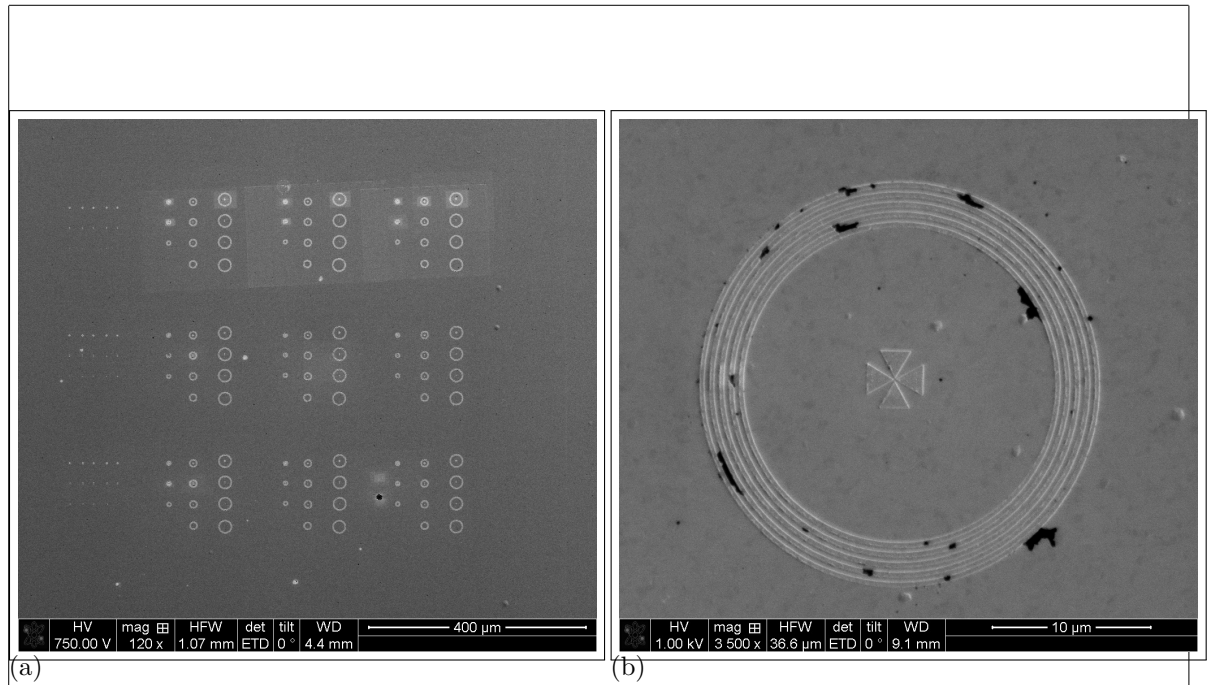


Figure 7: SEM images of the antenna structures. (a) Overview of a field of antenna structures exhibiting various dimensions. (b) Detail of one antenna structure. In the middle the double bowtie design is visible. The ring grating structure is surrounding it.

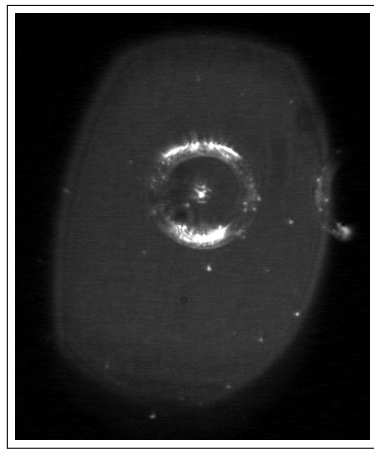


Figure 8: CCD image recorded in the confocal setup of an antenna structure under white light illumination. In the middle, the nanodiamond containing multiple SiV centers had been placed.

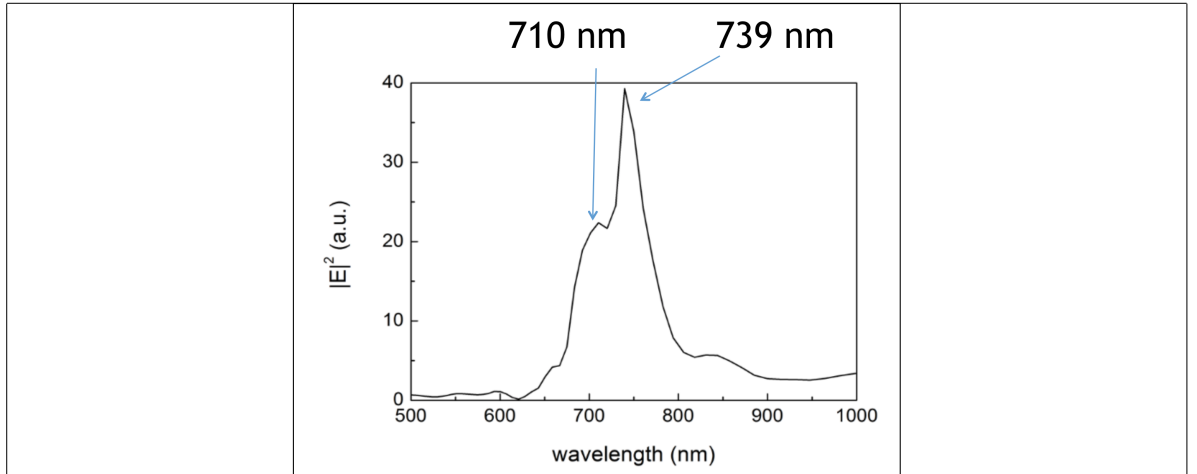


Figure 9: FDTD calculations of the electric field intensity as a function of wavelength in the gap of a double bowtie nanoantenna containing a nanodiamond.

0.2.2 Plasmonic Antenna Design

FDTD numerical simulations were performed using Lumerical software to characterize gold double bowtie nanoantennas on a gold substrate. The nanoantennas are tailored to have a gap of $g = 150$ nm (taking into account the diameter of the nanodiamonds of around 100 nm), side length of $L = 2\text{ }\mu\text{m}$, and a thickness of $t = 60$ nm (see Fig.3a). Upon excitation with incident light, an intense electromagnetic hotspot is formed in the nanoantenna gap [?], which is expected to excite a nanodiamond containing SiV centers aiming to enhance its fluorescence emission. Unlike a single bowtie that is sensitive only to the polarization along its principle axis (C₂ rotational symmetry), a double bowtie features a C₄ rotational symmetry and therefore focuses both parallel and perpendicular polarizations (i.e. all in-plane directions). The index of refraction of gold is taken from Palik [], and that of the nanodiamond is chosen to be $n = 2.4$ at $\lambda = 660$ nm. The electric field intensity in the nanoantenna gap is then measured as a function of wavelength to identify the antenna resonance. The spectrum is given in ?? where we observe that the resonance shows two peaks; an intense peak coinciding with the SiV emission wavelength ($\lambda = 739$ nm), and an additional mode at a lower wavelength ($\lambda = 710$ nm) [?] The resonance spectrum of the antenna alone shows only one peak at 739 nm. Thus, the additional peak is attributed to the presence of the nanodiamond that is slightly shifted from the center of the gap, corresponding to our experimental conditions. These calculations suggest, that the emission from an SiV center at 738 nm is effectively enhanced and directed by the antenna.

High optical confinement can be reached via successful SPP-LSP coupling at the nanoscale. One way of achieving that is by integrating diffraction gratings with nanoscale apertures or nanoantennas. Nanoantennas have shown to be very good candidates for focusing and enhancing electromagnetic fields in their vicinity. Nevertheless, due to their small size, a significant amount of the incident light is lost either by being scattered, reflected, or not entirely focused on the nanoantenna. On the other hand, plasmonic gratings act as sources for launching and orienting SPPs in a specific desired direction. Integrating a nanoantenna in the center of a concentric plasmonic ring grating creates a highly focused electromagnetic field at its center leading to an increase in the radiative decay rate as well as a collimated

read paper

Palik, E. D. Handbook of optical constants of solids. 3, (Academic press, 1998)

radiation of a dipole emitter placed inside [nancy::238–240] aus Nancys Doktorabreit al ERlaerung, warum die antenne ringe herum hat Optical plasmonic focusing has been extensively studied in the field of nanoplasmon- ics and has very important applications in high resolution imaging, sensing, waveg- uiding, nanolithography, and sub-wavelength optics. For this purpose, researchers have investigated several plasmonic structures capable of enhancing and confining surface plasmons into sub-wavelength dimensions. Cavities composed of diffraction gratings acting as SPP launchers can be used as efficient nanoscale focusing devices [243,244], confined surface plasmon polariton amplifiers [245], and fluorescence emission enhancement tools [246] (Fig. 4.1a). It has been shown that the plasmonic $\text{AIJ} \text{Bull}\ddot{\text{A}}\text{Zs Eye}$ structure, made of periodic concentric grooves in a metallic substrate, can lead to a strongly enhanced evanescent field focused in its center where propa- gating surface plasmons constructively interfere [247]. Controlling the directionality of transmitted light through an aperture surrounded by periodic corrugations was also achieved, which allows overcoming the limitations of low transmittance and high diffraction in the sub-wavelength regime [248]. In a similar study, the aperture is replaced by a narrow slit in the center of the Bull $\ddot{\text{A}}$ Zs Eye antenna leading to a higher power coupling, narrower radiated beam, and good return losses [249]. In addition, ring grating structures can be used to control the luminescence directivity of emitters placed in the center. Fluorescence beaming of molecules placed in a nanoaperture surrounded by concentric metallic grooves was studied by directing their emission in a precise direction and with a specific angular width depending on their wavelength [250]. Similar work related to the fluorescence emission of quan- tum dots placed in a slit surrounded by a ring grating shows that their emission can be manipulated to form perfectly narrow collimated beams [251] (Fig. 4.1b). Ring gratings surrounding diamond nanoposts [186] and circular diamond nanowires [135] with embedded nitrogen-vacancy (NV) centers were also used to improve the collec- tion efficiency and radiative decay rate of single NV centers. Directing the far-field emission of single NV centers placed in the center of a Bull $\ddot{\text{A}}$ Zs Eye grating was also recently investigated in a study that resulted in a high collection efficiency within a low numerical aperture [252]. This motivates us to use the ring grating structure described below to study efficient plasmon-emitter coupling at the nanoscale. An interesting property of the device is that the position of excitation determines the direction of propagation of the SPPs, providing a flexible mean of studying their interactions with molecules or dipole-like emitters placed on the surface.

fehlt
Erk-
laerung
zu Rin-
gen

0.2.3 SiV centers in a Plasmonic Double Bowtie Antenna

In the following, we discuss specific details and challenges concerning our initial attempts of coupling SiV centers to plasmonic double bowtie nanoantennas. Furthermore, we assert successful coupling and report spectroscopic measurements of an SiV center situated inside the gap of the antenna.

When transferring nanodiamonds to the center of an antenna, we distinguish between nanodiamonds hosting To transfer individual nanodiamonds hosting one or more SiV centers to the center of an antenna, we follow two approaches: First we chose a nanodiamond containing several SiV centers for pick-and-place and afterwards a nanodiamond containing a single SiV center. As mentioned before, single SiV centers may be damaged by the electron radiation in the SEM during pick-and-place and stop emitting photoluminescence light. Hence, we decided to run first experiments with nanodiamonds containing multiple SiV centers. This approach has the advantages that we are able to gain experience in the execution of the pick-and-place

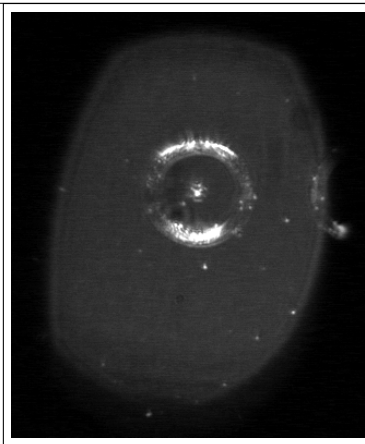


Figure 10: CCD image recorded in the confocal setup of an antenna structure under white light illumination. In the middle, the nanodiamond containing multiple SiV centers had been placed.

process without the risk of permanently damaging the emitter and therefore rendering the tedious pick-and-place process futile. For measurements of the intensity enhancement by the antenna, a single emitter is necessary. However, the antenna's influence on the SiV center spectrum can be studied when several emitters are present. Therefore, studies of the spectrum are performed in this first approach.

After we gained experience with the first approach, we searched for a suited nanodiamond containing a single SiV center. The aim was to perform saturation and second order correlation measurements to probe single SiV centers, and consequently quantify the exact Purcell enhancement imposed by the nanoantenna on a single photon emitter.

Nanodiamond With Multiple SiV centers Coupled to Antenna

The nanodiamonds exploited for the approach of coupling multiple SiV centers to an antenna were produced by a wet-milling process from a CVD diamond film¹. The solution of nanodiamonds which exhibit a median size of 100 nm were spin-coated on an iridium substrate treated with Piranha etch. To ensure that a pre-characterized nanodiamond exhibiting preferred optical properties (eg. narrow linewidth, high count rate) is later found again, the iridium substrate was engraved with reference cross markers produced by a focused ion beam prior to the spin-coating process. After spin-coating, the sample was placed in an oven for 3 hours at 450 °C to oxidize the surface and remove any residual graphite and amorphous carbon.

?? shows the spectrum recorded of the preselected nanodiamond. The ZPL peak exhibits a wavelength of 738.55(1) nm and a linewidth of 5.00(3) nm. These numbers correspond well to the ZPL of unstrained SiV centers and therefore allows us to deduce that the studied nanodiamond contains at least one SiV center. Photon autocorrelation measurements revealed, that the nanodiamond contains multiple SiV centers.

To determine the position of the nanodiamond on the original substrate, first a scan with a

¹wet-milling performed by A. Muzha, group of A. Krueger, Julius-Maximilians Universität Würzburg, diamond film grown by group of O. Williams, School of Engineering, Cardiff University

fehlergrenzen
verfünen
machen

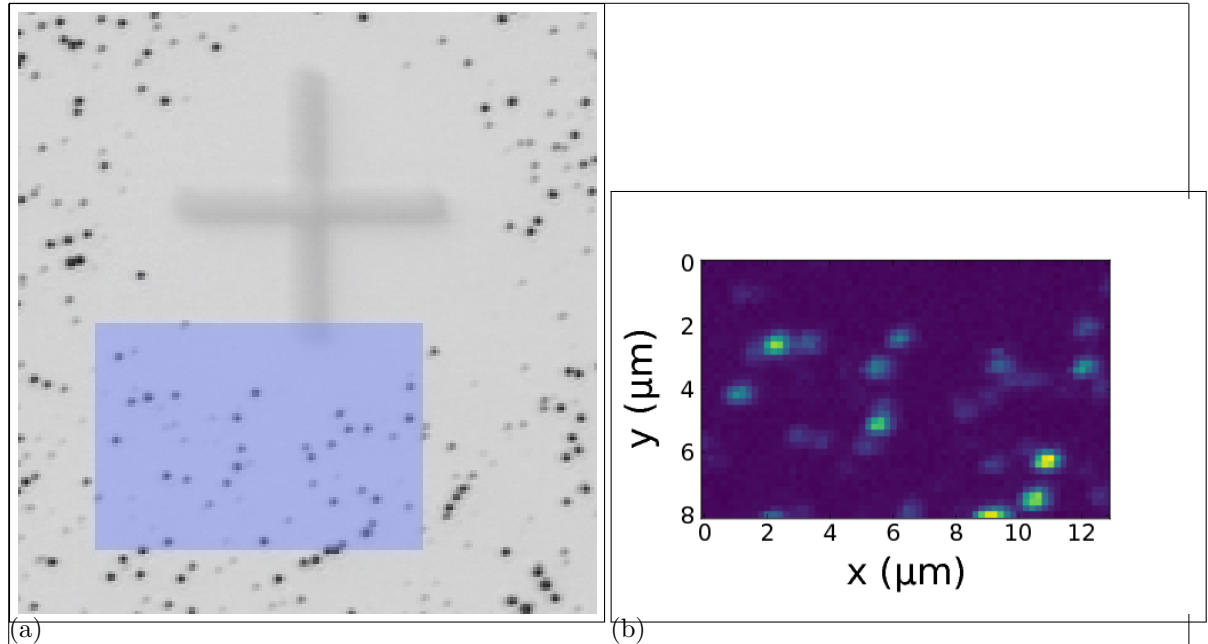


Figure 11: (a) Picture recorded with a commercial high resolution laser scanning microscope. The area shaded in blue represents the photoluminescence scan in image (b). (b) Photoluminescence scan of a $8 \mu\text{m} \times 13 \mu\text{m}$

commercial laser scanning microscope (LSM) was performed as described in ???. ?? shows a part of an obtained LSM image. The cross marker can easily be identified, the black dots are nanodiamonds. After transferring the sample into the confocal setup, confocal scans of the corresponding areas are performed (??). The area corresponding to the fluorescence light scan in ?? is shaded blue in ?? . When looking closely, the bright spots in the fluorescence light scan can be identified with nanodiamonds visible in ?? . The image in the SEM is very similar to the image obtained by the LSM. Therefore, once a nanodiamond containing a preselected emitter is identified in the LSM scan, it is easy to find the same emitter in the SEM.

The picking part of the pick-and-place process was performed in the same manner as described in the section about VCSELs (??). The gold surface of the plasmonic antenna caused a high adhesion between the antenna surface and the nanodiamond. Once the nanodiamond touched the gold, it could not be picked up again with the tungsten tip. The nanodiamond first touched the antenna structure a few nanometers away from the gap and immediately stuck to the surface, on top of one of the triangles. Therefore, the nanodiamond had to be pushed into the gap with the nanomanipulator tip. This process caused some damage to the antenna structure. The damage is visible as black area at the tip of the top triangle in ?? . However, FDTD simulations of damaged antennas reveal that this modification of the antenna hardly influences the antenna resonance.

After this deterministic placement, the antenna sample is placed in the confocal setup. The structure where the nanodiamond was placed is searched observing the sample surface in a CCD image under white light illumination (??). A scan of the antenna is performed in the confocal setup using the 660 nm continuous wave laser of the setup. The scan serves to locate the middle of the antenna structure and therefore the nanodiamond which had been placed there. An outline of the rings is visible in an overview scan of the antenna structure (??).

bild dazu

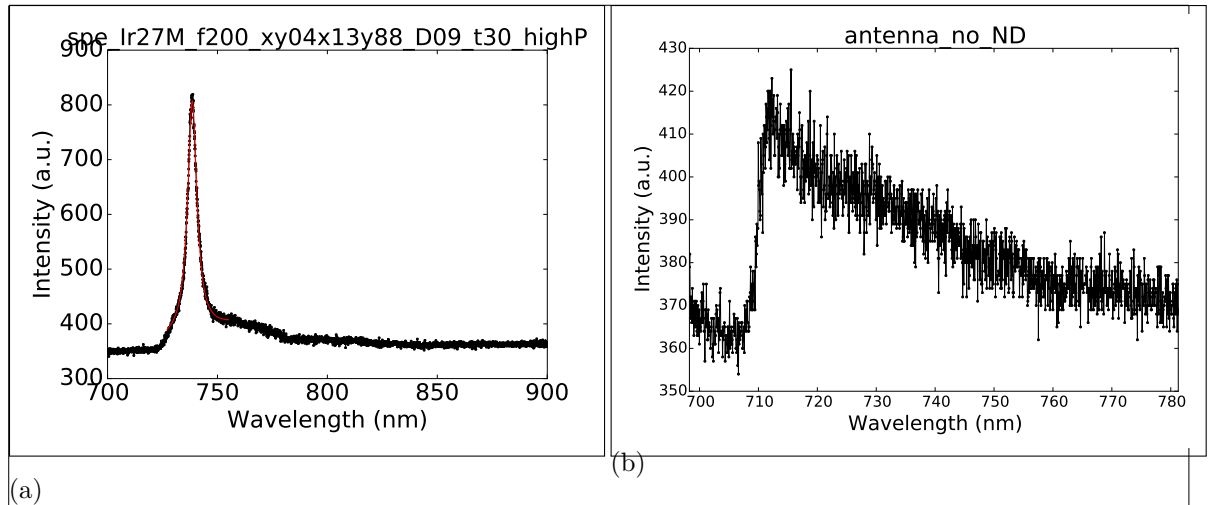


Figure 12: (a) PL spectrum of the emitter in the preselected nanodiamond at room temperature. Black: experimental results; red: fit to experimental data,

verfuenftige fehlergrenzen einfuegen

which yields a ZPL center wavelength of 738.55(1) nm and a linewidth of 5.09(3) nm

Zooming in to the middle of these rings, some of the edges of the bowtie antenna are vaguely visible (??). This images suffices to approach the nanodiamond close enough to measure a PL spectrum. The PL spectrum of the SiV center in the nanodiamond gives insight to the effect of the nanoantenna on its emission. The result is displayed in ?? . To rule out artifacts, a spectrum of an antenna of the same dimensions without nanodiamond is recorded (??). The additional peak at a lower wavelength is attributed to the antenna resonance mode. To verify this, we convolute the experimental PL spectrum of the nanodiamond measured before placing it in the nanoantenna (??) with the intensity spectrum of the nanoantenna obtained by simulations (??). The resulting spectrum is given in ?? , and is in good agreement with the measured spectrum in ?? , confirming that indeed the extra peak is due to the antenna resonance.

Nanodiamond With Single SiV center Coupled to Antenna

In this section, coupling a nanodiamond containing only few SiV centers to a double bowtie antenna is reported. The origin sample used for this experiment is an iridium substrate onto which a solution of nanodiamonds were drop-casted. Starting material for the nanodiamonds was a electronic grade diamond film produced by the company rho-BeSt coating (now CarbonCompetence). It was then milled in a bead-assisted sonic disintegration process² to nanodiamonds of a size of . The nanodiamonds were drop-casted at 60 °C onto an iridium substrate containing cross markers which had been treated with Piranha etch. Preselecting a nanodiamond with a single SiV center is imposes further constrains to the suitability of an nanodiamond. First, only a small percentage of the technically suited nanodiamonds (size, isolation) contain a single SiV center, second, damage due to electron radiation during pick-and-place. After an SiV center with a small dip in the $g^{(2)}$ function, indicating only few SiV

groesse
einfuegen

²A. Krueger, Julius-Maximilians Universität Würzburg

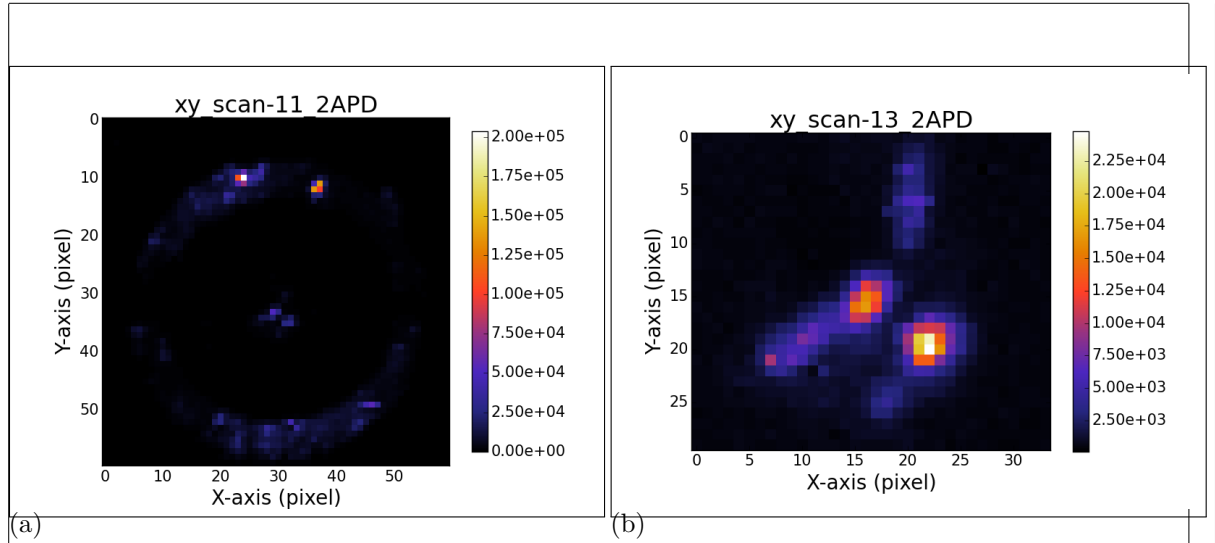


Figure 13: (a) Confocal scan of the double bowtie antenna where a nanodiamond containing multiple SiV centers had been placed. The rings are visible. (b) Detail scan of the triangles of the same antenna structure, which make up the double bowtie antenna. While the separate triangle cannot be seen, some edges and two bright spots are visible. To identify the place of the nanodiamond we compare the middle point of the rings in (a), the point of intersection of the edges and the bright spot and conclude that the upper bright spot in (b) is the location of the nanodiamond.

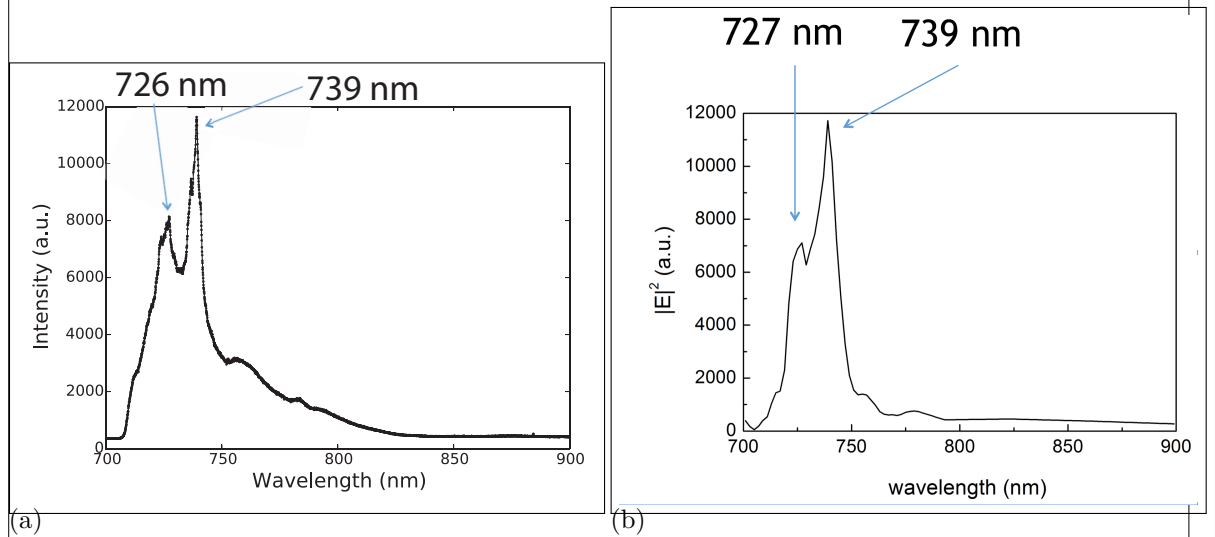


Figure 14: (a) Measured PL spectrum of the emitter after placing the nanodiamond into the nanoantenna, (b) Convolution of the spectrum of the measured PL spectrum of the emitter before pick-and-place (see Figure ??) and the simulated resonance spectrum of the nanoantenna (see Figure 9).

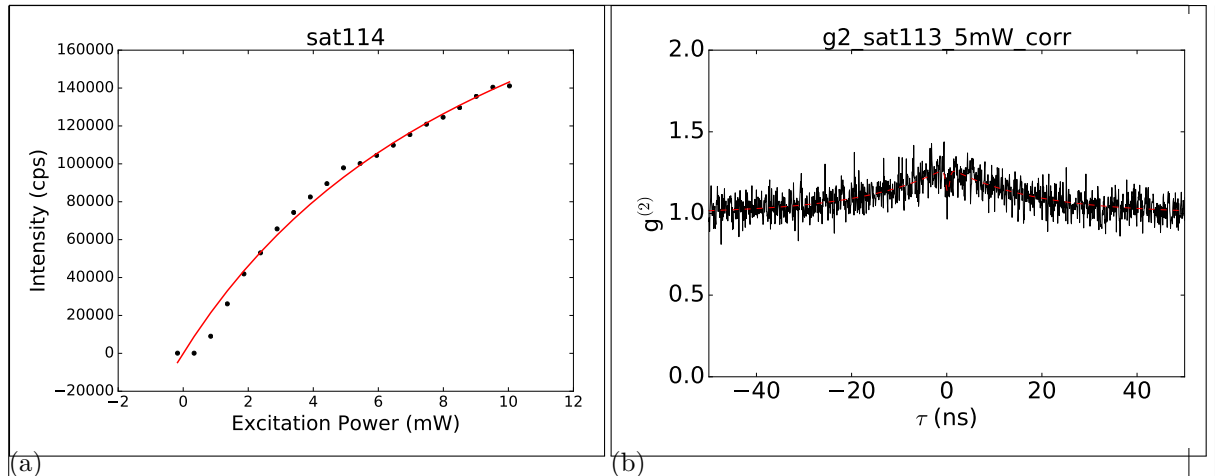


Figure 15: <caption>

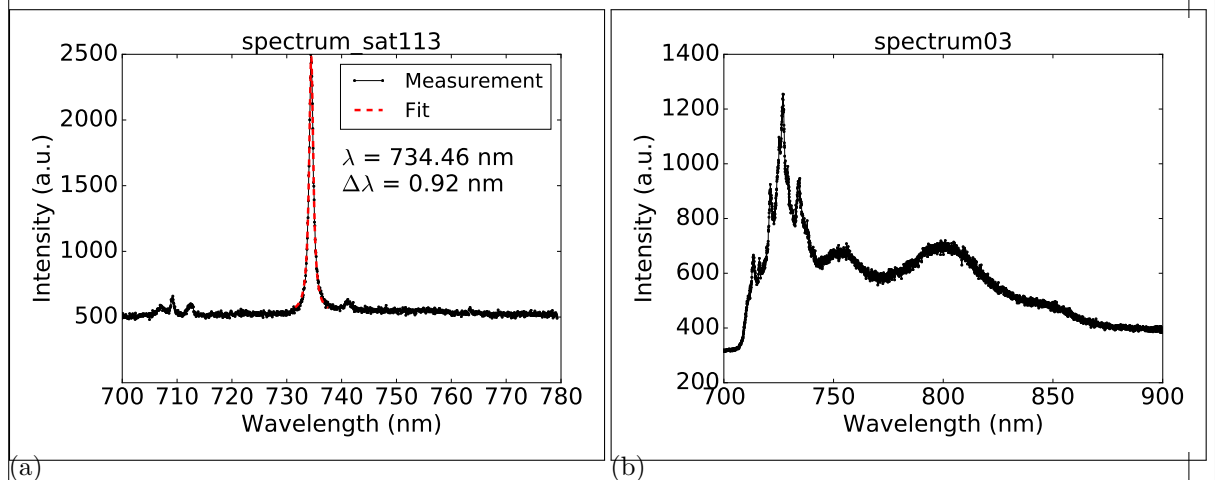


Figure 16: <caption>

centers.

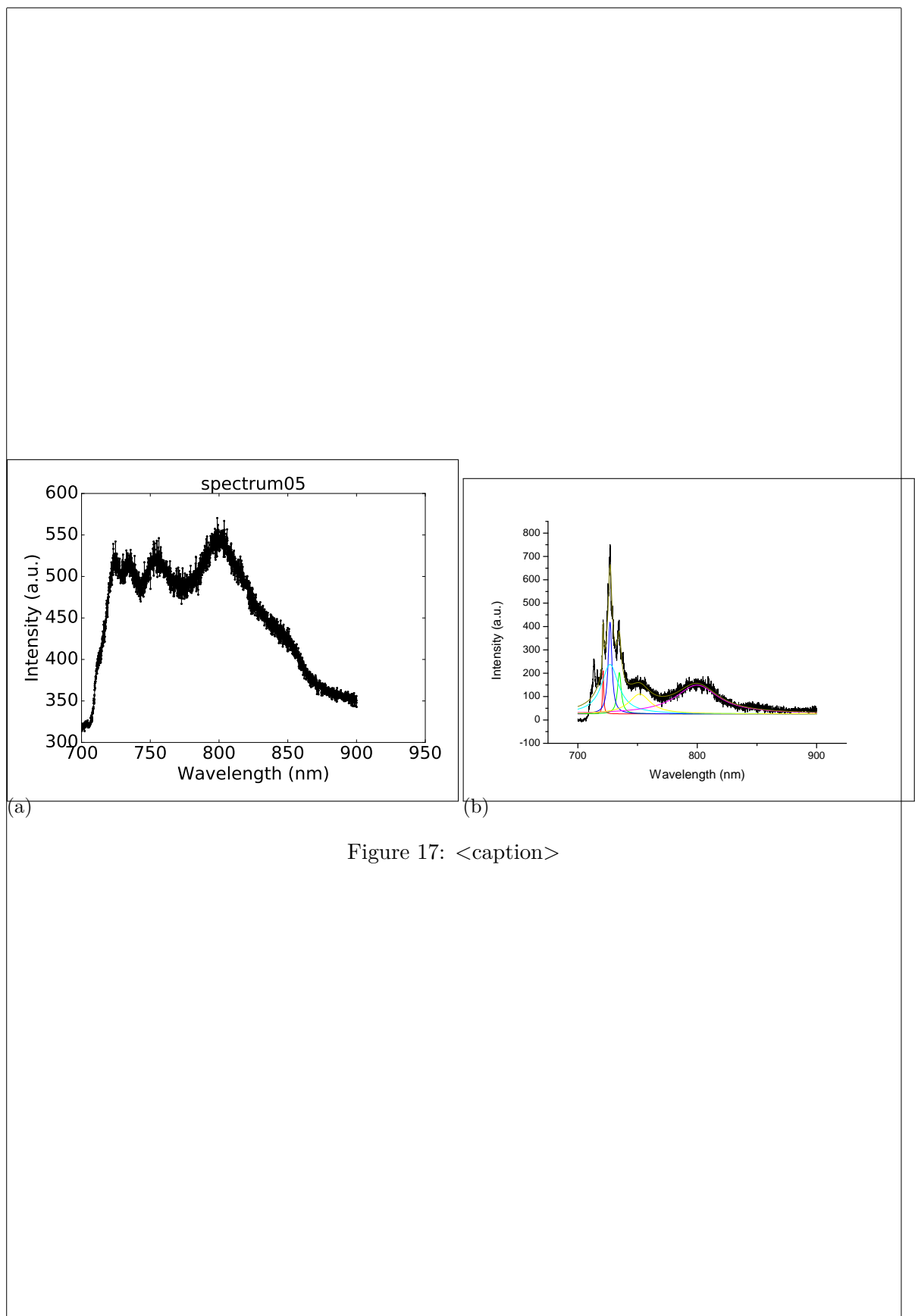


Figure 17: <caption>